

Exploiting Redundancy in Cartesian Impedance Control of UAVs Equipped with a Robotic Arm

Vincenzo Lippiello and Fabio Ruggiero

Abstract—A Cartesian impedance control for UAVs equipped with a robotic arm is presented in this paper. A dynamic relationship between generalized external forces acting on the structure and the system motion, which is specified in terms of Cartesian space coordinates, is provided. Through a suitable choice of such variables and with respect to a given task, thanks to the added degrees of freedom given by the robot arm attached to the UAV, it is possible to exploit the redundancy of the system so as to perform some useful subtasks. The hovering control of a quadrotor, equipped with a 3-DOF robotic arm and subject to contact forces and external disturbances acting on some points of the whole structure, is tested in a simulated case study.

I. INTRODUCTION

The latest years have seen a growing interest of the research community towards the field of aerial robotics. Unmanned aerial vehicles (UAVs) are often employed in several “passive” application scenarios such as inspection, remote sensing, surveillance and so on. Lately, these vehicles are used in “active” tasks such as grasping and manipulation.

Grabbing an object with a UAV during the flight arises several problems due to both the unstable dynamics of the vehicle and the coupling effects given by the presence of the object [1]. Hence, the gripper becomes a key feature in such a process, and thus even its design should be carefully taken into account [1], [2], [3].

The bigger the carried payload, the bigger should be the capacity of the single employed UAV. For this reason, an interesting approach is to use multiple collaborative UAVs in order to perform the transportation task [4]. The static equilibrium at a desired pose of a grasped payload and the consequent stability analysis are addressed in [5].

However, the complete switching from “passive” into “active” tasks requires mechanical structures in order to perform more complex actions. Mobile ground platforms [6], [7], underwater vehicles [8] and space robots [9] can be taken as examples of this scenario. Therefore, UAVs equipped with a robotic arm could be an efficient solution providing an aerial vehicle with the capability of performing dexterous manipulation tasks, but this is a still rather far adopted solution.

The research leading to these results has been supported by the AIRobots and ARCAS collaborative projects, which both have received funding from the European Communitys Seventh Framework Programme (FP7/2007-2013) under grant agreements ICT-248669 and ICT-287617, respectively. The authors are solely responsible for its content. It does not represent the opinion of the European Community and the Community is not responsible for any use that might be made of the information contained therein.

The authors are with PRISMA Lab, Dipartimento di Informatica e Sistemistica, Università degli Studi di Napoli Federico II, via Claudio 21, 80125, Naples, Italy {lippielo, fabio.ruggiero}@unina.it

Just as the presence of a carried object creates coupling effects in the dynamic model of the system, in the same way a mounted robot arm provides even more issues since its dynamics depend on the actual configuration of the whole state of the system. The dynamic model and control for classical robot manipulators are described in [10]. On the other hand, the dynamic models of different UAVs structures are provided in [11], [12], while tracking controls and stabilization are described in [12] and [13], respectively. Several other control strategies based on backstepping [14], optical flow [15], port Hamiltonian framework [16] and so on, can be found in the literature. Due to the high nonlinearity of the dynamic model of the single UAV, some components are often neglected, linearized or simplified. By assuming that the orientation dynamics of the UAV are compensated with separated high-gain control loop, a hierarchical control is usually considered [12], [17], and for which a time scale separation exists between the translational (slow time scale) and the rotational (fast time scale) dynamics. Under such assumption, a proportional and derivative controller is employed in [18] in order to stabilize the vehicle both in free flight and during contact. The gains are not changed in the switching between the two aforementioned conditions, but the boundaries of the displacements and the stiffnesses of the contact, approximated with a spring, are defined so as to achieve the goal.

The high complexity and coupling between the terms of the whole UAV plus robot arm dynamic model could not allow the separation between translation and orientation dynamics. In this paper, a Cartesian impedance control [19] is considered in order to realize a desired dynamical relationship between the whole system motion, specified in terms of coordinates in the Cartesian space, and generalized external forces acting on the structure. The contact is thus just represented with these general external forces while the Cartesian coordinates act as a mass-damper-spring system with respect to them, and where contact displacements and stiffnesses are imposed by the control law gains. Differently from [20], through a suitable choice of such Cartesian variables and with respect to a given task, it is possible to exploit the redundancy of the system thanks to the added degrees of freedom (DOF) given by the robot arm mounted on the UAV. In this way, some secondary tasks (subtasks) can be performed within a hierarchical framework, optimizing some given quality indices, e.g. manipulability, obstacles avoidance, joint limits, etc. The hovering control of a quadrotor, equipped with a 3-DOF robot arm and subject to contact forces and external disturbances acting on some

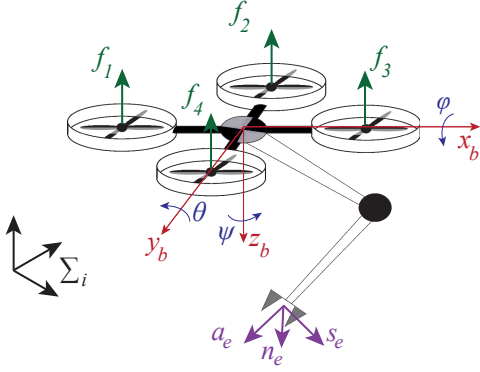


Fig. 1. UAV/Arm system illustration with the related reference frames.

points of the whole structure, is illustrated with a simulation case study.

II. MODELING

A. Kinematic model

With reference to the system depicted in Fig. 1, the equations describing the UAV position and attitude are those of a 6-DOF rotating rigid body. Let Σ_i be the world-fixed inertial reference frame and let Σ_b be the body-fixed reference frame placed at the vehicle center of mass. The absolute position of Σ_b with respect to Σ_i is denoted by $\mathbf{p}_b = [x \ y \ z]^T$, while the UAV attitude is described by the ZYX (in the current frame) set of yaw-pitch-roll Euler angles $\phi_b = [\psi \ \theta \ \varphi]^T$. Further, let $\dot{\mathbf{p}}_b$ denote the absolute linear velocity of the aerial vehicle, while $\dot{\mathbf{p}}_b^b$ describes the absolute linear velocity of the UAV with respect to Σ_b . On the other hand, let ω_b be the absolute rotational velocity of the aerial vehicle, while ω_b^b denotes the absolute rotational velocity of the UAV with respect to Σ_b . By denoting with $\dot{\phi}_b$ the time derivative of ϕ_b , the following equations can be introduced

$$\dot{\mathbf{p}}_b = \mathbf{R}_b \dot{\mathbf{p}}_b^b, \quad (1a)$$

$$\omega_b = \mathbf{T}_b \dot{\phi}_b, \quad (1b)$$

$$\omega_b^b = \mathbf{R}_b^T \omega_b = \mathbf{R}_b^T \mathbf{T}_b \dot{\phi}_b = \mathbf{Q} \dot{\phi}_b, \quad (1c)$$

where $\mathbf{R}_b \in \text{SO}(3)$ is the rotation matrix denoting the orientation of Σ_b with respect to Σ_i , \mathbf{T}_b is the (3×3) transformation matrix between the time derivative of ϕ and the correspondent ω_b , and $\mathbf{Q} = \mathbf{R}_b^T \mathbf{T}_b$ maps the time derivative of ϕ_b into the UAV angular velocity expressed with respect to Σ_b . It is worth noticing that the matrices above introduced suffer from the so-called *representation singularities* [10], that is $\theta \neq \pm k \frac{\pi}{2}$, with $k = 1, 3, 5, \dots$

Thereby, the direct kinematics of the UAV can be expressed by the following homogeneous transformation matrix

$$\mathbf{A}_b(\mathbf{p}_b, \phi_b) = \begin{bmatrix} \mathbf{R}_b & \mathbf{p}_b \\ \mathbf{0}^T & 1 \end{bmatrix}. \quad (2)$$

As shown in Fig. 1, a robotic manipulator is attached to the UAV. The following derivation about the kinematic and dynamic models of the system does not depend on the particular choice of where the manipulator is attached.



Fig. 2. Examples of UAVs endowed with a manipulator: on the left the ARCAS-project concept; on the right the AIRobots-project prototype.

Depending on the specific configuration, e.g. quadrotor, ducted-fan, and so on, the best mounting of the manipulator in order to have a self-stabilizing behavior will be considered (see Fig. 2). The arm consists of n rigid links connected by means of joints q_i , with $i = 1, \dots, n$. The end of the kinematic chain, that is not connected to the UAV basis, is an end-effector, e.g. a gripper. Hence, with respect to Σ_b , the direct kinematics function can be computed with the Denavit-Hartenberg convention [10], and it is expressed by the following homogeneous transformation matrix

$$\mathbf{A}_e^b(\mathbf{q}) = \begin{bmatrix} \mathbf{n}_e^b(\mathbf{q}) & \mathbf{s}_e^b(\mathbf{q}) & \mathbf{a}_e^b(\mathbf{q}) & \mathbf{p}_e^b(\mathbf{q}) \\ 0 & 0 & 0 & 1 \end{bmatrix}, \quad (3)$$

where \mathbf{q} is the $(n \times 1)$ vector of joint variables, $\mathbf{n}_e^b, \mathbf{b}_e^b, \mathbf{a}_e^b$ are the unit vectors of a frame attached to the end-effector, and \mathbf{p}_e^b is the position vector of the origin of such a frame with respect to Σ_b . By combining (2) and (3), it is possible to obtain the absolute pose of the manipulator

$$\mathbf{A}_e(\boldsymbol{\xi}) = \mathbf{A}_b \mathbf{A}_e^b, \quad (4)$$

where $\boldsymbol{\xi} = [\mathbf{p}_b^T \ \phi_b^T \ q_1 \ \dots \ q_n]^T$ is the generalized joints vector of $n_\xi = 6 + n$ components. The expressions in (2) and (4) represent the configuration of the whole system (UAV plus arm) with respect to Σ_i .

Let $\dot{\mathbf{p}}_e$ and ω_e be the linear and angular velocities of the end-effector with respect to Σ_i , respectively, and let the vector $\mathbf{v} = [\dot{\mathbf{p}}_e^T \ \omega_e^T \ \dot{\mathbf{p}}_e^T \ \omega_e^T]^T$ collect the absolute linear and angular velocities of both the UAV and the manipulator end-effector. The mapping between \mathbf{v} and the time derivative of the generalized joints vector $\boldsymbol{\xi}$ is given by

$$\mathbf{v} = \mathbf{J} \dot{\boldsymbol{\xi}},$$

where the $(12 \times n_\xi)$ matrix \mathbf{J} is the so-called geometric Jacobian of the system, whose expression in this case is

$$\mathbf{J} = \text{diag}(\mathbf{I}_3, \mathbf{T}_b, \tilde{\mathbf{R}}_b \mathbf{J}_e^b),$$

in which \mathbf{I}_α denotes the $(\alpha \times \alpha)$ identity matrix, $\tilde{\mathbf{R}}_b = \text{diag}(\mathbf{R}_b, \mathbf{R}_b)$ and \mathbf{J}_e^b is the manipulator geometric Jacobian referred to Σ_b [10].

If the orientation of the manipulator is expressed in terms of a minimal representation ϕ_e , the direct kinematics equation can be also written in the following form

$$\mathbf{x} = \mathbf{k}(\boldsymbol{\xi}),$$

where $\mathbf{k}(\cdot)$ is an $(m \times 1)$ vector function, nonlinear in general, and \mathbf{x} is an $(m \times 1)$ vector describing the system configuration through a minimal representation of the orientation.

The linear mapping between the time derivative of \boldsymbol{x} and $\dot{\boldsymbol{\xi}}$ is given by

$$\dot{\boldsymbol{x}} = \boldsymbol{J}_a \dot{\boldsymbol{\xi}}, \quad (5)$$

where the $(m \times n_\xi)$ matrix \boldsymbol{J}_a is the so-called analytical Jacobian of the system, derived via differentiation of $\boldsymbol{k}(\cdot)$. Since the function $\boldsymbol{k}(\cdot)$ is not usually available in a direct form, specially for the orientation part, but requires the computation of the elements of the relative rotation matrices, it is possible to compute a relationship between \boldsymbol{J} and \boldsymbol{J}_a by exploiting the equations in (1) and by considering similar equations for the angular velocity of the robot end-effector.

B. Dynamic model

The dynamic model of the whole UAV plus robotic arm system can be derived by considering the *Euler-Lagrange formulation*: more details are available in [20].

The system dynamics can be hence written as follows:

$$\boldsymbol{B}(\boldsymbol{\xi})\ddot{\boldsymbol{\xi}} + \boldsymbol{C}(\boldsymbol{\xi}, \dot{\boldsymbol{\xi}})\dot{\boldsymbol{\xi}} + \boldsymbol{g}(\boldsymbol{\xi}) = \boldsymbol{u} + \boldsymbol{u}_{ext}, \quad (6)$$

in which the $(n_\xi \times 1)$ vector \boldsymbol{u} represents the generalized input forces, \boldsymbol{g} is a $(n_\xi \times 1)$ vector of gravitational terms, \boldsymbol{B} is an $(n_\xi \times n_\xi)$ symmetric and positive definite inertia matrix and \boldsymbol{C} is a suitable $(n_\xi \times n_\xi)$ matrix whose generic element is

$$c_{ij} = \sum_{k=1}^{n_\xi} \frac{1}{2} \left(\frac{\partial b_{ij}}{\partial \xi_k} + \frac{\partial b_{ik}}{\partial \xi_j} + \frac{\partial b_{jk}}{\partial \xi_i} \right) \dot{\xi}_k,$$

where b_{ij} is the generic element of $\boldsymbol{B}(\boldsymbol{\xi})$, with $i, j = 1, \dots, n_\xi$. The last term \boldsymbol{u}_{ext} in (6) shapes the effects of generalized external forces at the joint level.

In the quadrotor case of Fig. 1, by supposing negligible the aerodynamic effects and by supposing low-speed displacements [12], the vector \boldsymbol{u} has the following expression

$$\boldsymbol{u} = \bar{\boldsymbol{R}}_b \boldsymbol{N} \boldsymbol{f} = \boldsymbol{\Xi} \boldsymbol{f}, \quad (7)$$

where $\boldsymbol{f} = [\boldsymbol{f}_v^T \quad \boldsymbol{\tau}^T]^T$, with \boldsymbol{f}_v the (4×1) input vector of forces given by the quadrotor motors and $\boldsymbol{\tau}$ the $(n \times 1)$ input vector of the manipulator joint torques. Moreover, $\bar{\boldsymbol{R}}_b = \text{diag}(\boldsymbol{R}_b, \boldsymbol{Q}^T, \boldsymbol{I}_n)$ is an $(n_\xi \times n_\xi)$ matrix, and $\boldsymbol{N} = \text{diag}(\boldsymbol{\Omega}, \boldsymbol{I}_n)$ is an $(n_\xi \times 4 + n)$ matrix, in which

$$\boldsymbol{\Omega} = \begin{bmatrix} 0 & 0 & 0 & 0 \\ 0 & 0 & 0 & 0 \\ 1 & 1 & 1 & 1 \\ 0 & d & 0 & -d \\ -d & 0 & d & 0 \\ c & -c & c & -c \end{bmatrix},$$

where d is the distance from a motor to the center of the vehicle and $c > 0$ is the drag factor. By noticing that $\boldsymbol{\Xi}^T \boldsymbol{\Xi}$ is always invertible, except for the aforementioned representation singularity, it is possible to invert the relationship in (7) yielding $\boldsymbol{f} = \boldsymbol{\Xi}^\dagger \boldsymbol{u} + \boldsymbol{f}_N$, where the symbol \dagger denotes the generalized pseudo-inversion of a matrix, and \boldsymbol{f}_N is a vector of generalized forces of both the UAV and the manipulator. Hence, belonging \boldsymbol{f}_N to the null space of $\boldsymbol{\Xi}$, it does not give any contribution to \boldsymbol{u} and thus to the dynamic motion

equations. For this reason, only the input vector \boldsymbol{u} will be considered in the remainder of the paper.

III. CARTESIAN IMPEDANCE CONTROL

Impedance control is often employed in robot manipulation tasks, while its use in aerial robotics is still rather far. The goal of impedance control is to realize a particular desired dynamical relationship between the motion of the UAV plus the robotic arm and external forces. Usually, classical impedance controllers require the measurements of external forces, which typically act on the manipulator end-effector [21]. This situation is unfeasible in aerial robotics applications since other disturbances and unmodelled aerodynamic effects can arise during the performed task. Hence, the method proposed in [19] can be revised in such a context.

A. Non-redundant case

Consider a vector of Cartesian coordinates \boldsymbol{x} with $m = n_\xi$. With this choice, the Jacobian \boldsymbol{J}_a has $(n_\xi \times n_\xi)$ dimensions. Deriving (5) with respect to time yields

$$\ddot{\boldsymbol{x}} = \boldsymbol{J}_a \ddot{\boldsymbol{\xi}} + \dot{\boldsymbol{J}}_a \dot{\boldsymbol{\xi}}. \quad (8)$$

Let \boldsymbol{x}_d , $\dot{\boldsymbol{x}}_d$ and $\ddot{\boldsymbol{x}}_d$ be the desired, even time-varying, desired *virtual* position, velocity and acceleration, respectively. The word *virtual* is used since this desired configuration will be reached only along the unconstrained motion directions due to the presence of external forces. By denoting with $\tilde{\boldsymbol{x}} = \boldsymbol{x}_d - \boldsymbol{x}$ the actual position error, the following control law can be defined

$$\boldsymbol{u} = \boldsymbol{g} + \boldsymbol{J}_a^T (\boldsymbol{B}_x \ddot{\boldsymbol{x}}_d + \boldsymbol{C}_x \dot{\boldsymbol{x}}_d + \boldsymbol{K}_D \dot{\tilde{\boldsymbol{x}}} + \boldsymbol{K}_P \tilde{\boldsymbol{x}}), \quad (9)$$

where \boldsymbol{K}_P and \boldsymbol{K}_D are $(n_\xi \times n_\xi)$ symmetric and positive definite matrices, while \boldsymbol{B}_x and \boldsymbol{C}_x are the inertia and Coriolis matrices with respect to the \boldsymbol{x} variables and defined as follows

$$\begin{aligned} \boldsymbol{B}_x &= \boldsymbol{J}_a(\boldsymbol{\xi})^{-T} \boldsymbol{B}(\boldsymbol{\xi}) \boldsymbol{J}_a(\boldsymbol{\xi})^{-1} \\ \boldsymbol{C}_x &= \boldsymbol{J}_a(\boldsymbol{\xi})^{-T} \left(\boldsymbol{C}(\boldsymbol{\xi}, \dot{\boldsymbol{\xi}}) - \boldsymbol{B}(\boldsymbol{\xi}) \boldsymbol{J}_a(\boldsymbol{\xi})^{-1} \dot{\boldsymbol{J}}_a(\boldsymbol{\xi}) \right) \boldsymbol{J}_a(\boldsymbol{\xi})^{-1}. \end{aligned}$$

By substituting (9) into (6), and by taking into account (5) and (8), the equations describing the closed-loop behaviour, and hence the desired dynamic relationship in terms of a mass-damper-spring system, namely are

$$\boldsymbol{B}_x \ddot{\tilde{\boldsymbol{x}}} + (\boldsymbol{C}_x + \boldsymbol{K}_D) \dot{\tilde{\boldsymbol{x}}} + \boldsymbol{K}_P \tilde{\boldsymbol{x}} = \boldsymbol{f}_{ext}, \quad (10)$$

where the $(n_\xi \times 1)$ vector \boldsymbol{f}_{ext} shapes the effects of generalized external forces at the Cartesian coordinate level. A way to choose the gains \boldsymbol{K}_P , that corresponds to the stiffness, and \boldsymbol{K}_D , that defines the damping, is described in [19]. In particular, \boldsymbol{K}_D should be a function of $\boldsymbol{\xi}$ in order to take into account the change of \boldsymbol{B}_x during time.

It is worth noticing that in case of regulation control problems, i.e. $\dot{\boldsymbol{x}}_d = \mathbf{0}$, the effort for computing (9) drastically reduces, and the system (10) becomes a passive mapping between \boldsymbol{f}_{ext} and $\dot{\tilde{\boldsymbol{x}}}$.

The presented control law requires the inversion of \mathbf{J}_a that strongly relies on the particular choice of the vector \mathbf{x} . The structure of a UAV with an attached robotic arm presents coupled terms in the Cartesian variables, as it can be noticed by examining (4). Thereby, it is not easy to choose $m = n_\xi$ independent variables in order to obtain a full-rank matrix \mathbf{J}_a . Much easier is to choose a number of independent coordinates $m < n_\xi$ that only partly specify the configuration of the whole system.

B. Redundant case

By choosing now an $(m \times 1)$ vector \mathbf{x} , with $m < n_\xi$, the Jacobian matrix \mathbf{J}_a in (5) becomes a rectangular matrix with rank m in the considered working space. The remaining $n_\xi - m$ coordinates can be employed in the so-called *nullspace motion* that does not affect the motion of the chosen \mathbf{x} variables, but that can be exploited in order to optimize some secondary tasks.

The superposition principle for impedance [21] provides a method in order to combine different behaviors. Hence the control input can now be defined as

$$\mathbf{u} = \mathbf{u}_c + \mathbf{P}\mathbf{u}_N, \quad (11)$$

where \mathbf{u}_c is taken as in (9) so as to obtain the same closed loop system of (10), while \mathbf{P} is an $(n_\xi \times n_\xi)$ matrix that projects \mathbf{u}_N onto the nullspace of \mathbf{J}_a^T in order not to distort the primary task, and \mathbf{u}_N is referred to as the nullspace impedance exploited so as to satisfy as much as possible other subtasks. Notice that if more subtasks have to be fulfilled, a hierarchical priority approach can be defined in (11) through the formalism presented in [22].

A generic secondary task can be defined as

$$\boldsymbol{\sigma} = \mathbf{f}_\sigma(\boldsymbol{\xi}), \quad (12)$$

where $\boldsymbol{\sigma}$ is a $(m_\sigma \times 1)$ vector of variables to be controlled, that are a function of the generalized joints $\boldsymbol{\xi}$. The desired values $\boldsymbol{\sigma}_d$ are obtained for a given configuration $\boldsymbol{\xi}_{d,0}$. It should be noted that such desired configuration of the variables should be equal to the ones obtained in the desired virtual Cartesian configuration \mathbf{x}_d . This means that $\mathbf{k}(\boldsymbol{\xi}_{d,0}) = \mathbf{x}_d$. If the subtask is not designed in such a way, it is not possible to statically reach both the desired Cartesian position and the nullspace configuration simultaneously.

Deriving (12) with respect to time yields

$$\dot{\boldsymbol{\sigma}} = \frac{\partial \mathbf{f}_\sigma}{\partial \boldsymbol{\xi}} \dot{\boldsymbol{\xi}} = \mathbf{J}_\sigma(\boldsymbol{\xi}) \dot{\boldsymbol{\xi}},$$

where \mathbf{J}_σ is the $(m_\sigma \times n_\xi)$ Jacobian matrix of the task. Considering only the regulation case for the given subtask, by defining with $\mathbf{e}_N = \boldsymbol{\sigma}_d - \boldsymbol{\sigma}$ the subtask error, the following control law can be designed for the \mathbf{u}_N term in (11)

$$\mathbf{u}_N = \mathbf{J}_\sigma^\dagger \mathbf{K}_{P_\sigma} \mathbf{e}_N + \mathbf{K}_{D_\sigma} \dot{\boldsymbol{\xi}}, \quad (13)$$

where \mathbf{K}_{P_σ} is an $(m_\sigma \times m_\sigma)$ gain matrix and \mathbf{K}_{D_σ} is an $(n_\xi \times n_\xi)$ damping matrix, added to damp out the oscillations of such nullspace term.

Notice that the particular choice of $\boldsymbol{\sigma} = \boldsymbol{\xi}$ in (12) yields the case presented in [19] that is

$$\mathbf{u}_N = \mathbf{K}_{P_\sigma} (\boldsymbol{\xi}_{d,0} - \boldsymbol{\xi}) + \mathbf{K}_{D_\sigma} \dot{\boldsymbol{\xi}},$$

where now both \mathbf{K}_{P_σ} and \mathbf{K}_{D_σ} are two $(n_\xi \times n_\xi)$ symmetric positive definite matrices representing the desired nullspace stiffness and damping, respectively.

Finally, a particular choice of \mathbf{P} is the so-called dynamically consistent projection matrix [21]

$$\mathbf{P} = \mathbf{I}_{n_\xi} - \mathbf{J}_a^T \left(\mathbf{J}_a \mathbf{B}^{-1} \mathbf{J}_a^T \right)^{-1} \mathbf{J}_a \mathbf{B}^{-1},$$

which gives some advantages in the nullspace term stability analysis.

IV. SIMULATION RESULTS

In this section the results of dynamic simulations performed through the MATLAB/SIMULINK environment are presented. With reference to the schematic representation of Fig. 1, the dynamic model of an ASCTEC PELICAN quadrotor with mass $m_b = 2$ kg and inertia matrix $\mathbf{H}_b = \text{diag}(1.24, 1.24, 2.48)$ m²kg has been derived. A 3-DOF robotic arm mounted at the bottom of the quadrotor is considered. The robotic manipulator is composed of 2 links and 3 revolute joints; in particular, the first two axes intersect in a common point. The two links are 15 cm and 5 cm length, respectively, while the corresponding centers of mass are located at the middle of each link. The mass and the inertia around the rotational axis for the first link are 0.049 kg and 0.0011 m²kg, respectively, while for the second link are 0.05 kg and 1.25e⁻⁴ m²kg. These values have been retrieved by building such a manipulator into a 3D CAD environment. Finally, a distance of 0.1 m, along the vertical axis z_b of Σ_b , is present between the center of Σ_b and the spherical joint reference frame. The initial values of the system generalized joints are set to $\boldsymbol{\xi} = [0 \ 0 \ 2 \ 0 \ 0 \ 0 \ -\pi/2 \ 0 \ \pi/2]^T$.

Two case studies, namely A and B, will be presented. In both of them, the Cartesian variables chosen for the control are the absolute orientation of the vehicle and the position of the manipulator end-effector, i.e. $\mathbf{x} = [\phi_b^T \ \mathbf{p}_e^T]^T$. With this choice, it could be shown that \mathbf{J}_a has always row-rank 6, except for the case of the aforementioned representation singularities. The initial value of \mathbf{x} is set to $[0 \ 0 \ 0 \ 0 \ -0.5 \ 1.75]^T$ for both cases. The proposed controllers have been implemented with a sampling time of 1 ms and both simulations have a duration of 10 s.

A. Case study A

In this case study, an external force acts along the \mathbf{x}_b axis of Σ_b (see Fig. 3(a)). This simulates windy or unmodeled situations during an hovering control action. Such a force has a magnitude of 1 N, and it is applied at $t_1 = 1$ s and ends after 1 s, while another force of the same magnitude is applied along the same direction at $t_2 = 3.5$ s and ends after 1.5 s.

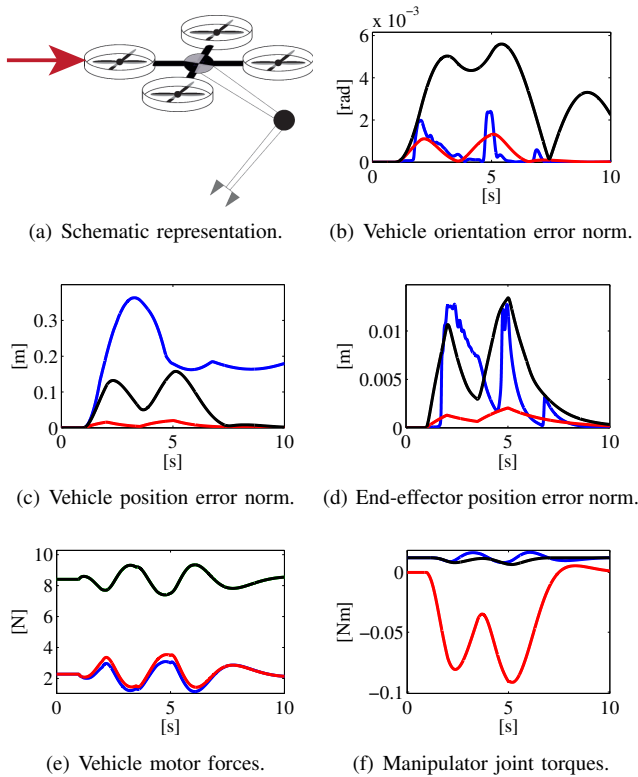


Fig. 3. Case study A. The color legend in subfigures (b)-(d) is: blue, rigid system without exploiting redundancy; red, rigid system exploiting redundancy; black, compliant system exploiting redundancy. Subfigures (e)-(f) show the time histories of the generalized forces of both the vehicle and the manipulator only in the compliant behaviour case. The color legend in subfigure (e) is: blue, green, red and black represent forces related to vehicle motors 1, 2, 3 and 4, respectively. Notice that the black line hides the green one. The color legend in subfigure (f) is: blue, red and black represent the torques of manipulator joints 1, 2 and 3, respectively.

First, a rigid behavior has been set in \mathbf{u}_c in (11), with $\mathbf{K}_p = 100\mathbf{I}_6$. On the other hand, in order to choose \mathbf{K}_D , the values of the damping ratio for each component have been tuned to 0.8, so as not to have oscillations. The results of this simulation, with the nullspace control law \mathbf{u}_N set to zero, are shown in blue in Figs. 3(b)-3(e). Hence, the system reacts to the external forces with a high stiffness, as it can be noticed in Fig. 3(b) and Fig. 3(d) by the small norm error with respect to the considered Cartesian variables \mathbf{x} . However, without including the redundancy management, the position of the vehicle cannot be directly controlled, but it is coupled with the other variables through the direct kinematic equations (4). As it can be noticed in Fig. 3(c), the vehicle does not accomplish the hovering task since it moves, in norm, of about 0.35 m with respect its initial position, mainly along the \mathbf{x}_b direction where the external force acts.

Therefore, a rigid behavior of the system exploiting redundancy is investigated. In order to fully accomplish a hovering task, the desired subtask is to maintain the vehicle position at the initial condition, that is $\boldsymbol{\sigma} = [0 \ 0 \ 2]^T - \mathbf{p}_b$. The stiffness matrix in \mathbf{u}_c has been tuned to $\mathbf{K}_p = 5\mathbf{I}_6$, while the damping ratio values are equal to the previous case. The matrices \mathbf{K}_{P_σ} and \mathbf{K}_{D_σ} in (13) have been set to \mathbf{I}_3 and \mathbf{I}_9 , respectively. The results of this simulation

are shown in red in Figs. 3(b)-3(e). In particular, Fig. 3(c) shows how the vehicle does not move any more from its initial position. Despite the fact that the stiffness gains are lower than the previous case, even the error norm about the vehicle orientation (see Fig. 3(b)) and the end-effector position (see Fig. 3(d)) are better than the previous case, thanks to the coupled terms. This underlines the importance about managing such secondary tasks.

Finally, a compliant behavior of the system exploiting redundancy is investigated. The desired subtask is the same as before, but now the stiffness matrix in \mathbf{u}_c has been tuned to $\mathbf{K}_p = \mathbf{I}_6$, while the damping ratio values are 0.2 for each component. The matrices \mathbf{K}_{P_σ} and \mathbf{K}_{D_σ} in (13) have been set to $0.1\mathbf{I}_3$ and $0.1\mathbf{I}_9$, respectively. The results of this simulation are shown in black in Figs. 3(b)-3(e). The compliant behavior is noticed by looking at the increased values of the error norms in each time history. After the effect of the external force is vanished, the system recovers the desired conditions. Moreover, in this last case, the time histories of the vehicle input forces and the joints input torques are depicted in Fig. 3(e) and Fig. 3(f), respectively. The values for the manipulator joint torques are kept down and this is suitable for the small motors employed in the arm to contain the weight. For what concerns the vehicle forces, the maximum value is about 10 N and this is also reasonable with respect to commercial quadrotors. The time histories of the input generalized forces for the other two previous cases have not been reported for brevity, but the maximum values do not exceed the ones here reported.

B. Case study B

In this case study, an external force acts along the \mathbf{x}_b axis of Σ_b with the same aforementioned modality. In addition, another force with 0.5 N of magnitude acts along the \mathbf{a}_e end-effector axis for all the simulation time (see Fig. 4(a)). This scenario simulates the case of the manipulator end-effector in contact with a wall, while the aerial vehicle should again deal with windy situations. Thereby, the manipulator end-effector position is chosen to be rigid, while the quadrotor orientation is chosen to be compliant. Hence, the stiffness matrix in \mathbf{u}_c has been tuned to $\mathbf{K}_p = \text{diag}(\mathbf{I}_3, 5\mathbf{I}_3)$, while the damping ratio values are 0.2 for the UAV orientation components and 0.8 for the arm end-effector ones. The desired subtask is to maintain the vehicle position at the initial condition and optimize a *manipulability measure* of the robotic arm. In particular, the second link should always have a relative position of 90 degrees with respect to the first link. Hence, the subtask definition is $\boldsymbol{\sigma} = [0 \ 0 \ 2 \ \pi/2]^T - [\mathbf{p}_b^T \ q_3]^T$. The matrices \mathbf{K}_{P_σ} and \mathbf{K}_{D_σ} in (13) have been set to $\text{diag}(0.1\mathbf{I}_3, 1)$ and \mathbf{I}_9 , respectively.

The results of this simulation are shown in Figs. 4(b)-4(e). The imposed high stiffness limits the oscillations of the position of the manipulator end-effector (see Fig.4(d)). Since the contact force at the arm end-effector is always present, the Cartesian components errors can be zeroed only along the unconstrained directions. On the other hand, the compliance behavior imposed to the orientation variables

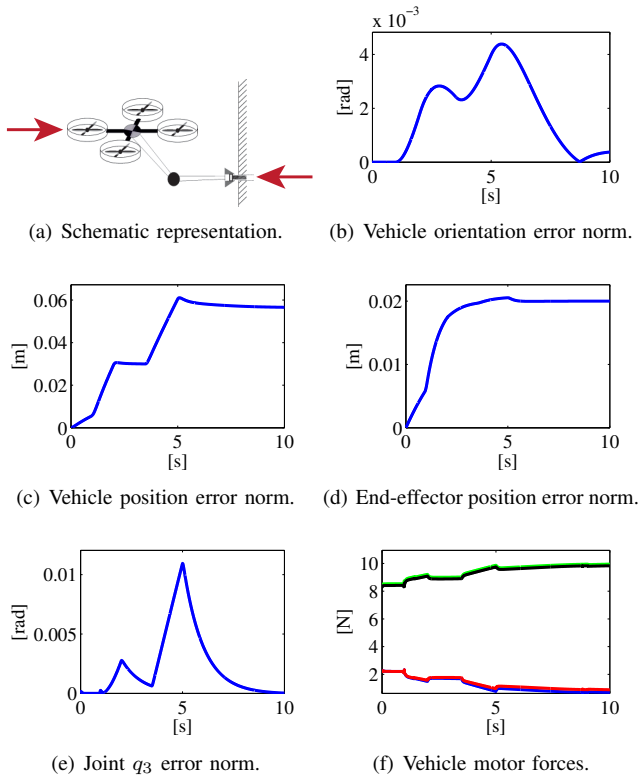


Fig. 4. Case study B. Subfigure (f) shows the time histories of the vehicle generalized forces. The corresponding color legend is: blue, green, red and black represent the forces related to vehicle motors 1, 2, 3 and 4, respectively.

of the quadrotor can be observed in Fig. 4(b), while the manipulability secondary task is fulfilled as it could be seen in Fig. 4(e). On the other hand, the small first three values of \mathbf{K}_{D_σ} denote a compliant behavior also for the vehicle position. This is evident by looking at Fig. 4(c) where the position is slowly recovering its initial condition, i.e. the error is slowly reaching the null value. The vehicle input forces are depicted in Fig. 4(f) and they are in line with the considerations made for the case study A. The manipulator joint torques are not shown for brevity, but they still maintain small values as in the previous case study.

V. CONCLUSION AND FUTURE WORK

A dynamic relationship between the UAV plus robotic arm system motion and generalized external forces acting on the structure has been derived through a Cartesian impedance control. The whole system redundancy, with respect to a given task, has been exploited through a suitable choice of variables in the Cartesian space. The possibility to accomplish some other subtasks has been tested in simulation.

Future work will be focused on the definition of more complex subtasks which could be useful in aerial manipulation applications. Moreover, a deep analysis of the dynamic model of the whole system could guide the construction of light-weight robotic arms suitable in such aerial manipulation scenarios, even with the presence of flexible elements.

REFERENCES

- [1] P. Pounds, D. Bersak, and A. Dollar, "Grasping from the air: Hovering capture and load stability," in *2011 IEEE International Conference on Robotics and Automation*, (Shanghai, CN), pp. 2491–2498, 2011.
- [2] V. Ghadiok, J. Goldin, and W. Ren, "Autonomous indoor aerial gripping using a quadrotor," in *2011 IEEE/RSJ International Conference on Intelligent Robots and Systems*, (San Francisco, CA), pp. 4645–4651, 2011.
- [3] D. Mellinger, Q. Lindsey, M. Shomin, and V. Kumar, "Design, modelling, estimation and control for aerial grasping and manipulation," in *2011 IEEE/RSJ International Conference on Intelligent Robots and Systems*, (San Francisco, CA), pp. 2668–2673, 2011.
- [4] I. Maza, J. Kondak, M. Bernard, and A. Ollero, "Multi-UAV cooperation and control for load transportation and deployment," *Journal of Intelligent and Robotics Systems*, vol. 57, no. 1, pp. 417–449, 2010.
- [5] N. Michael, J. Fink, and V. Kumar, "Cooperative manipulation and transportation with aerial robots," in *Autonomous robots. Special issue: Robotics: Science and Systems* (R. Tedrake and Y. Matsuoka, eds.), vol. 30, pp. 73–86, 2011.
- [6] Y. Yamamoto and X. Yun, "Coordinating locomotion and manipulation of a mobile manipulator," *IEEE Transactions on Automatic Control*, vol. 39, no. 6, pp. 1326–1332, 1994.
- [7] C. Korpela, T. Danko, and P. Oh, "MM-UAV: Mobile manipulating unmanned aerial vehicle," *Journal of Intelligent and Robotics Systems*, vol. 65, no. 1, pp. 93–101, 2012.
- [8] G. Antonelli, *Underwater Robotics. Motion and Force Control of Vehicle-Manipulator Systems*, vol. 2 of *Springer Tracts in Advanced Robotics*. Berlin Heidelberg, D: Springer-Verlag, 2006.
- [9] K. Yoshida and B. Wilcox, "Space robots and systems," in *Springer Handbook of Robotics* (B. Siciliano and O. Khatib, eds.), pp. 1031–1063, Springer, 2008.
- [10] B. Siciliano, L. Sciacivco, L. Villani, and G. Oriolo, *Robotics. Modelling, planning and control*. London, UK: Springer-Verlag, 2009.
- [11] T. Cheviron, A. Chriette, and F. Plestan, "Generic nonlinear model of reduced scale UAVs," in *2009 IEEE International Conference on Robotics and Automation*, (Kobe, J), pp. 3271–3276, 2009.
- [12] K. Nonami, F. Kendoul, S. Suzuki, W. Wang, and D. Nakazawa, *Autonomous Flying Robots. Unmanned Aerial Vehicles and Micro Aerial Vehicles*. Springer, 2010.
- [13] P. Castillo, R. Lozano, and A. Dzul, "Stabilization of a mini rotorcraft with four rotors," *IEEE Control Systems Magazine*, vol. 25, no. 6, pp. 45–55, 2005.
- [14] T. Madani and A. Benallegue, "Sliding mode observer and backstepping control for a quadrotor unmanned aerial vehicles," in *Proceedings of the 2007 American Control Conference*, (New York City, NY), pp. 5887–5892, 2007.
- [15] V. Lippiello, G. Loianno, and B. Siciliano, "MAV indoor navigation based on a closed-form solution for absolute scale velocity estimation using optical flow and inertial data," in *50th IEEE Conference on Decision Control and European Control Conference*, (Orlando, FL), pp. 3566–3571, 2011.
- [16] R. Mahony, S. Stramigioli, and J. Trumpf, "Vision based control of aerial robotic vehicles using the port Hamiltonian framework," in *50th IEEE Conference on Decision Control and European Control Conference*, (Orlando, FL), pp. 3526–3532, 2011.
- [17] R. Mahony and T. Hamel, "Robust trajectory tracking for a scale model autonomous helicopter," *International Journal of Robust and Nonlinear Control*, vol. 14, no. 12, pp. 1035–1059, 2004.
- [18] P. Pounds and A. Dollar, "UAV rotorcraft in compliant contact: Stability analysis and simulation," in *2011 IEEE/RSJ International Conference on Intelligent Robots and Systems*, (San Francisco, CA), pp. 2660–2667, 2011.
- [19] C. Ott, *Cartesian Impedance Control of Redundant and Flexible-Joint Robots*, vol. 49 of *Springer Tracts in Advanced Robotics*. Berlin Heidelberg, D: Springer-Verlag, 2008.
- [20] V. Lippiello and F. Ruggiero, "Cartesian impedance control of a UAV with a robotic arm," in *10th International IFAC Symposium on Robot Control*, (Dubrovnik, HR), 2012.
- [21] B. Siciliano and L. Villani, *Robot Force Control*. Kluwer Academic Publishers, 1999.
- [22] G. Antonelli, "Stability analysis for prioritized closed-loop inverse kinematic algorithms for redundant robotic systems," *IEEE Transactions on Robotics*, vol. 25, no. 5, pp. 985–994, 2009.